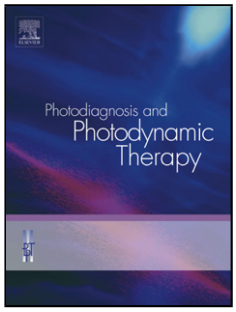

Title: Classification of Dental Diseases Using Hyperspectral Imaging and Laser Induced Fluorescence

Authors: Ahmed L. Abdel Gawad, Yasser El-Sharkawy, H.S. Ayoub, Ashraf F. El-Sherif, Mahmoud F. Hassan

PII: S1572-1000(18)30258-8
DOI: https://doi.org/10.1016/j.pdpdt.2018.11.017
Reference: PDPDT 1298

To appear in: *Photodiagnosis and Photodynamic Therapy*

Received date: 10 August 2018
Revised date: 15 November 2018
Accepted date: 26 November 2018

Please cite this article as: Abdel Gawad AL, El-Sharkawy Y, Ayoub HS, El-Sherif AF, Hassan MF, Classification of Dental Diseases Using Hyperspectral Imaging and Laser Induced Fluorescence, *Photodiagnosis and Photodynamic Therapy* (2018), https://doi.org/10.1016/j.pdpdt.2018.11.017

Classification of Dental Diseases Using Hyperspectral Imaging and Laser Induced Fluorescence

Ahmed L. Abdel Gawad[1], Yasser El-Sharkawy[2], H.S. Ayoub[3] Ashraf F. El-Sherif[4], and Mahmoud F. Hassan[5]

[1,] Medical Service Department, Egyptian Armed Forces, Cairo, Egypt
[2]Department of Biomedical Engineering, Military Technical College, Cairo, Egypt
[3]Department of Physics, Faculty of Science, Cairo University, Egypt
[4,5] Laser Photonics Research Center, Engineering Physics Department, Military Technical College, Cairo, Egypt

Highlights

- Employing Fluorescence hyperspectral imaging system to discriminate between tooth classes.
- Obtaining series of wavelengths, noting each lesion individually.
- Tooth lesions have either dark or bright appearance at estimated wavelengths.
- New laser wavelength 395-nm was able to identify white spot and root calculus.

ABSTRACT

Purpose: Early diagnosis of tooth demineralization, and enamel, dentin caries lesions, present a valuable solution to avoid or decrease their deleterious effect. The aim of this study was to design a simple, effective, and non-invasive technique, employing a novel laser wavelength to classify and differentiate between various tooth abnormalities in-vitro, by estimating wavelengths, showing distinctive appearance for each tooth class.

Methods: This study implies a fluorescence hyperspectral imaging system employing a 395-nm laser diode source, irradiating a pre-diagnosed 12 molars and premolars teeth. The obtained reconstructed images were displayed and processed by HSAnalysis2XL, accompanied by a custom made digital, and image signal processing algorithms, revealing the exact wavelengths, characterizing the fluorescence of each tooth pre-diagnosed class.

Results: The proposed hyperspectral imaging system was able to discriminate between normal, and abnormal dental classes for the entire specimens. Furthermore, a series of wavelengths, noting each lesion individually were obtained from the spectroscopic hyperspectral output. The root calculus, white spot,

dentin caries, and enamel caries have a bright visual appearance at λ_3 = 702 nm, λ_5 = 771 nm, and λ_6 = 798 nm respectively. Consequently, these abnormalities exhibit a dark appearance at λ_1 = 421 nm, λ_2 = 462 nm, and λ_4 = 734 nm. The wavelength selections were confirmed by the grayscale image outcomes.

Conclusions: This study provides a set of wavelengths that can be employed by dentists in the future to diagnose white spot, root calculus, and enamel, dentin caries lesions under the irradiation of a new UV-Visible laser illumination source without, any hazardous thermal or mechanical effects.

.

Keywords: Demineralization**;** Caries detection; Fluorescence Spectroscopy; Hyperspectral Imaging; Lesion Classification.

INTRODUCTION

Human teeth are considered as one of the main body mineralized tissues. , It can be anatomically described by an upper part noted as the crown, and one or more roots imbedded in the lower part of the teeth [1]. The main constituent mineralized layers of the tooth are the enamel and dentin layers, their main functions are to protect and support the tooth to its surroundings [2]. Sound tooth is constituted of 5 surfaces, namely the buccal which faces or is toward the cheeks, lingual surface or toward the roof of the mouth or tongue, while the mesial surface is the closest to the midline of the mouth, while distal surface is the farthest from midline of the mouth, last but not least the occlusal surface which is the chewing surface of the tool [3].

Dental Caries is regarded as one of the most widespread oral diseases affecting 60 to 90% of the schoolchildren, as well as, most of the adults [4]. Regardless of the great awareness about dental healthcare and oral hygiene, it still remains the major reason for oral pain and tooth loss worldwide [5]. Dental caries is a dynamic disease recognized by the demineralization of tooth enamel, causing an increase in the enamel surface porosity, commonly called white spots due to its increased refractive index [6]. Till that stage, caries can be contained and reversed with non-invasive remineralization treatments, such as fluoride and anti-bacterial therapies, or irradiation by a low level laser beam [7, 8]. Yet if the early enamel caries is left untreated, it may lead to a great damage of the underlying dental tissues, at that point an invasive intervention is needed to restore the damaged tooth, or the possibility of tooth loss becomes enormous. Hence, to avoid these deleterious outcomes, an early detection regime for the initial demineralization stages is required for aiding in the assessment and monitoring of caries progress results, as well as, the applied treatments effectiveness [9].

Non-invasive diagnostic tools, including visual inspection tactile, aided by radiographs are commonly used by dentist from half a century till nowadays. Those are simple and easy to use techniques, albeit are sometimes unreliable, and present hazardous effects, as patients are exposed to ionized radiation. Both procedures lack of sensitivity and specificity warrant for the development of other early detection tools of

caries lesion formation and progression [10, 11]. Optical and imaging based methods have been lately increasingly applied for the early detection of caries lesions. Opto-imaging methods have the advantage of being a non-destructive, non-hazardous techniques, with minimal thermal and mechanical damage to the dental tissue. Moreover, it can detect early demineralization events based on the dental morphological changes, caused by bacterial bio-waste, which initiate the demineralization process [12, 13]. Polarized Raman spectroscopy, multiphoton imaging, infrared tomography, photoacoustic, optical coherence tomography (OCT), and terahertz imaging presents the new optical and laser potential imaging tools for the early demineralization detection [14-16]. Most of these existing optical techniques depend on the light transport changes within the tooth, such as absorption, scattering, diffuse reflectance, and fluorescence. Dark areas such as stains, calculus, and progressed stages of caries tends to absorb the incident light, while porous areas such as white spots scatters, reflects light more than sound areas. Based on the patterns formed by light scattering away, or absorbed by the lesion with respect to the sound areas, a qualitative diagnostic technique evolved, called (FOTI) Fiber-optic trans illumination [17, 18], followed by digital imaging fiber-optic trans illumination (DIFOTI) technique was developed to enhance the sensitivity of the (FOTI) method in detecting incipient caries. Nevertheless, both techniques still suffer from significant limitations to be quantifiable due to the uneven light distribution inside the tooth, where the enamel and dentin layers exhibits high absorption and scattering [19]. To overcome such limitations, other detection methods based on fluorescence phenomenon were developed. These methods are the laser induced fluorescence (LIF), and quantitative laser induced fluorescence (QLF). Fluorescence spectroscopy technique is a non-invasive, non-ionized probing process, showing both high sensitivity and specificity. This technique is based upon the fluorescence phenomenon, arising from the interaction of the irradiating wavelength with the intrinsic endogenous fluorophores present in the sound enamel and dentin layers of the illuminated tooth sample, causing its excitation, and ultimately leading to the emission of higher wavelength [20, 21]. Consequently, the existing fluorophores in the enamel and dentin, exhibit a laser induced fluorescence (LIF), when excited by shorter visible laser wavelengths [22]. Moreover, the presence of exogenous fluorophores, owing to metallo-, copro-, and protoporphyrins of bacteria, as well as, bacterial metabolites, porphyrins and also possibly extrinsic and intrinsic polysaccharides in the caries cavity, and calculus also emits fluorescence [23, 24]. The increased scattering and absorption of the incident light on the tooth sample, derived by the caries progress process, could be measured and quantified by applying advanced fluorescence spectroscopic and hyperspectral imaging techniques[25].

DIAGNOdent. and VistaProof are considered to be the most commonly used commercial devices based on the laser fluorescence technology for the early detection of caries and its degree of severity. DIAGNOdent. is a device which utilizes red light laser for fluorescence excitation, causing the caries lesion to fluoresce more than the sound tissues, with the limitation of detecting the initial enamel lesion. Similarly, VistaProof

is a device which uses fluorescence camera to obtain a stream of life images, resulting from fluorescence irradiation by a blue laser of 405 nm. Unlike the DIAGNOdent device, the sound enamel fluorescence more than diseased areas enabling the monitoring of caries lesion evolution. Nevertheless, both suffers from obtaining only output static measurements, in addition to weak correlations with histological examinations [26] .

Hyperspectral imaging is another newly evolved medical imaging procedure that provides simultaneous accurate spatial and spectral information about a tissue or organ regarding the patient tissue sample, or disease in more than one spectral range. It has the potential to improve the fields of medical diagnostics and clinical research, by offering an accurate spectral information related to the tissue sample, or different disease conditions. Also, it is able to overcome the drawbacks of other conventional imaging techniques, and point spectroscopy [27].

A major goal of this work was to present a topology spectral map for the classification of healthy and diseased dental lesion classes, throughout the differentiation between those classes spatially and spectrally convectively. A custom non-invasive setup is employed utilizing a 395-nm laser diode source, and a SOC710 hyperspectral camera. Laser induced fluorescence(LIF) of the examined tooth sample was detected and measured by the visible hyperspectral imaging powerful camera. The hypercube output was used to obtain a set of wavelengths characterizing each of the pre-diagnosed dental lesions discretely.

Materials and methods

Twelve teeth samples were clinically diagnosed and classified using visual tactile method. Sound enamel, and dentine were marked, as well as, other dental abnormalities including, white spot, enamel caries, dentin caries, and root calculus. Each diagnosed tooth sample was optically imaged from the diagnosed surface, mostly the mesial one by a custom designed hyperspectral imaging system, utilizing a SOC710 hyperspectral camera (Fig. 1). The designed hyperspectral imaging system consists of a UV-Visible 395 nm violet laser, used to irradiate the sample under test, obtaining a spectroscopy measurement (one-dimensional 1-D) noting the pixel intensity at various wavelengths, together with a grayscale image (two-dimensional 2-D) noting the fluorescence emission of the entire spectroscopic dataset at the chosen wavelength, and an RGB (three dimensional 3-D) representing the hypercube image. Those hyperspectral camera outcomes are presented and are further displayed by the supported hyperspectral camera HSAnalysis2XL software. Outcomes can then be digitized and imaged signal processed by pre-designed algorithm, using MATLAB software.

Sample Preparation

Twelve molars, and pre-molars tooth samples, freshly extracted for different medical and dental reasons with no restorations, from adult patients different ages, were collected from a nearby educational dental hospital. Those teeth were either sound or infected by different degrees of caries, and other dental abnormalities. For standardization, all of the collected samples were diseased in the tooth mesial surface. The extracted tooth samples were immediately immersed, in Na-Cl solution (0.9%), mixed with (5%) of thymol to prevent dehydration, and then stored in sealed cups at room temperature. Prior to hyperspectral imaging measurements, which usually took place after utmost a week from extraction. Tooth samples were taken out of the preserving solution and washed in running tap water, brushed softly to get rid of food particles and blood residuals and then dried using a tissue paper. Afterwards, teeth were clinically examined by only one experienced consultant practitioner dentist and were mainly classified according to the visual tactile, aided by the International Caries Detection & Assessment System(ICDAS) as a reference guide using a microscope of 200x zoom capabilities. This clinical classification procedure took place after removing the cementum from the root to expose the dentin layer, without affecting other much affecting dental disorders. A written report was provided for the diagnosis, and classification of each sample individually, describing the exact position and the lesion class. Finally, tooth samples were centrally positioned in plastic transparent square cubes filled of wax, ensuring a fixed position for the tooth during hyperspectral imaging acquisition.

Experimental Setup

The hyperspectral imaging system (Fig. 1), consists of a laser diode source emitting a pencil beam of 395-nm light (FVLD-395-2), with nominal output power of 10 mW. A beam expander (THORLABS, model GBE20-A) was used to expand the pencil beam light from the violet laser source, to assure a normal distribution of light over the entire tooth. The expanded light is transmitted to the tooth under test by a 90° quartz prism from (Edmond Optics), which is utilized in the mid-way between the output expanded light and the sample for the purpose of re-directing the laser beam, as well as minimizing the axial path difference between the camera axis and the laser axis. In addition of, decreasing the dissipated power of light over the entire tooth sample, moreover to avoid intensity saturation of the image. A hyperspectral camera of type (SOC710) from (Surface Optics Cooperation, San Diego, CA, USA) was used to collect the reflected light from the surface of the sample, mostly due to fluorescence, and diffuse reflectance. The SOC710 hyperspectral camera is specified by a 128-spectral image per second at 12- bit resolution, 520 pixels per row, up to 33 rows per second, covering the visible and NIR spectral range from 400 – 1000 nanometer.

The reconstructed raw images captured by the hyperspectral camera are displayed on the Pc screen through a pre-installed camera software. The HSAnalysis2XL is a software utilized for the pre-processing of captured cubic images from the point of view of digital and image signal processing. The software

introduces an output raw data, in the form of spectroscopic measurements (1-D), grayscale (2-D), and hypercube (3-D) datasets that can be used to classify and discriminate between different classes of tooth lesion spatially and spectrally. The 1-D hypercube outcome, which represent the intensity of each image pixel at various wavelengths was then digitally processed by normalizing, and applying logarithmic function on the raw data. Targeting the presentation of the main wavelengths, discriminating between different pre-classified abnormalities. The estimated wavelengths are then reused to obtain the hypercube 2-D images noting those abnormality classes for further processing, and enhancement by the pre-designed image signal algorithms.

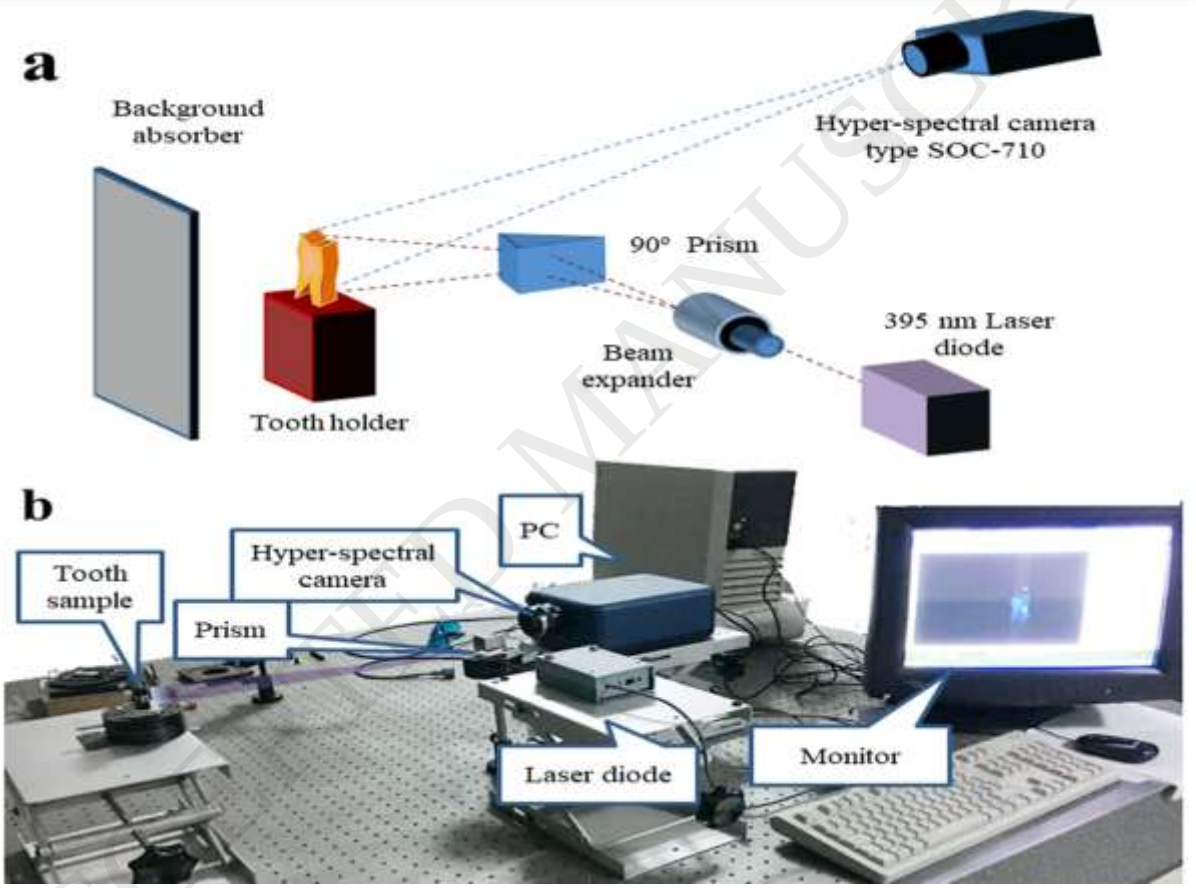

Fig. 1 Hyperspectral imaging system setup. a Schematic illustration. b Actual lab image.

Experimental Procedure

Hyperspectral Pre-Measurements

Before carrying out the hyperspectral imaging measurements, a dark frame is obtained in the absence of laser beam irradiation, and with the camera cap closing the iris, for the purpose of eliminating any present electronic system noise. Furthermore, a calibration frame was acquired, through using a white Halon panel, placed exactly instead of the examined sample in the presence of the laser irradiation, and with the camera

iris free of cap. Those frames were essentially for the HSAnalysis2XL software to obtain the absolute reflectance values of pixels for an image. Afterwards, a series of cubic images were taken for the samples under examination by the custom designed hyperspectral imaging system (Fig. 1). The collected cubes were then displayed by the HSAnalysis2XL software from which several outcomes can be obtained. Spectroscopic measurement 1-D representing the intensity for each pixel of the image versus the wavelength, together with a 2-D outcome showing a grayscale image of the cube at the selected wavelength for further processing, as well as, an RGB, and infra-red RGB images representing the spatial and spectral representations of the 3-D hypercube output images. The intended 1-D hypercube dataset, characterizing each dental class individually consist of a number of pixel intensities at various wavelengths, representing each of the pre-diagnosed abnormality chosen according to the diagnosis of the specialized dentist, and under his direct supervision for precise choices. For each dental lesion class, the 1-D data series of the characterizing pixel intensities were averaged, saved for the 12 tooth samples to be illustrated as raw data (Fig. 2). In order to obtain the absolute reflectance values of the pixel intensity for each tooth phenotype, the 1-D data series are subtracted from the dark frame, and then normalized by dividing it by the product of subtracting the calibration frame from the dark frame. While, the 2-D image was saved at the selected wavelengths after being subtracted from the dark frame, for further processing, and inspection.

Results

The scope of the results focuses on the hypercube outcomes representing, the one-dimensional spectroscopic measurements, and the grayscale two dimensional images obtained at deduced wavelengths.

A. Hyperspectral one-dimension outcomes

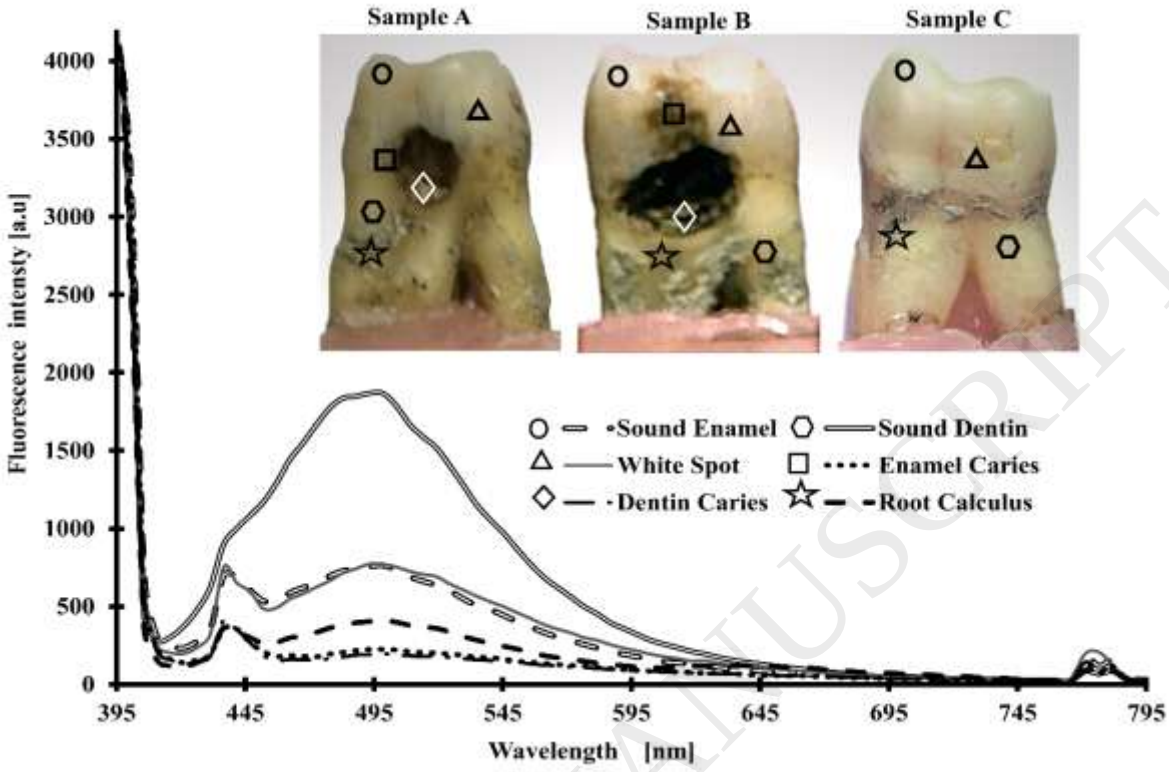

Fig. 2 Fluorograph of selected dental samples illuminated by 395nm laser beam

The one-dimensional spectroscopic measurements yielded from the hyperspectral imaging setup (Fig. 1), revealed both normal and abnormal tooth classes, as noted on the visible photos for the shown three exemplar samples (Fig. 2). The selected modeled photo samples consisted of sample A, and B, which display a molar tooth diseased by white spot, enamel and dentin caries, as well as, root calculus. While sample C was only diagnosed by white spot and root calculus, in which all of the presented samples are diseased in the mesial surface. The demonstrated raw data curve resulting from averaging the selected pre-diagnosed pixels demonstrating the six tooth classes for the entire set of tooth specimen, showed an acceptable discrimination between normal, and abnormal cases clearly at specific wavelengths (Fig. 2).

Clearly, the excitation wavelength shows a maximum peak at 395-nm, while the fluorescence spectra of the sound enamel and dentin tissues exhibit a narrow peak centered around 420-nm, as well as, a broad emission of maximum intensity around 500 nm, with an extended tail reaching the red and infra-red spectrum region. Obviously, spectra of the non-cavitated and cavitated caries, and root calculus, manifested the same behavior of the sound tissues with less intensity, and a slight wavelength shift for its peaks in comparison with sound layer ones. Moreover, an additional low fluorescence intensity peaks centered at 771-nm, 776-nm, and 782-nm, in which, the intensity of the 4 abnormality classes rule over that of the sound enamel and dentin classes. Consequently, the fluorescence intensity curve of the 4 abnormality

classes was found to be lower than that of the sound classes for the entire visible region. Whilst, in the far visible, near infra-red spectrum, the white spot and root calculus lesions manifest a greater fluorescence intensity spectral than sound enamel and dentin.

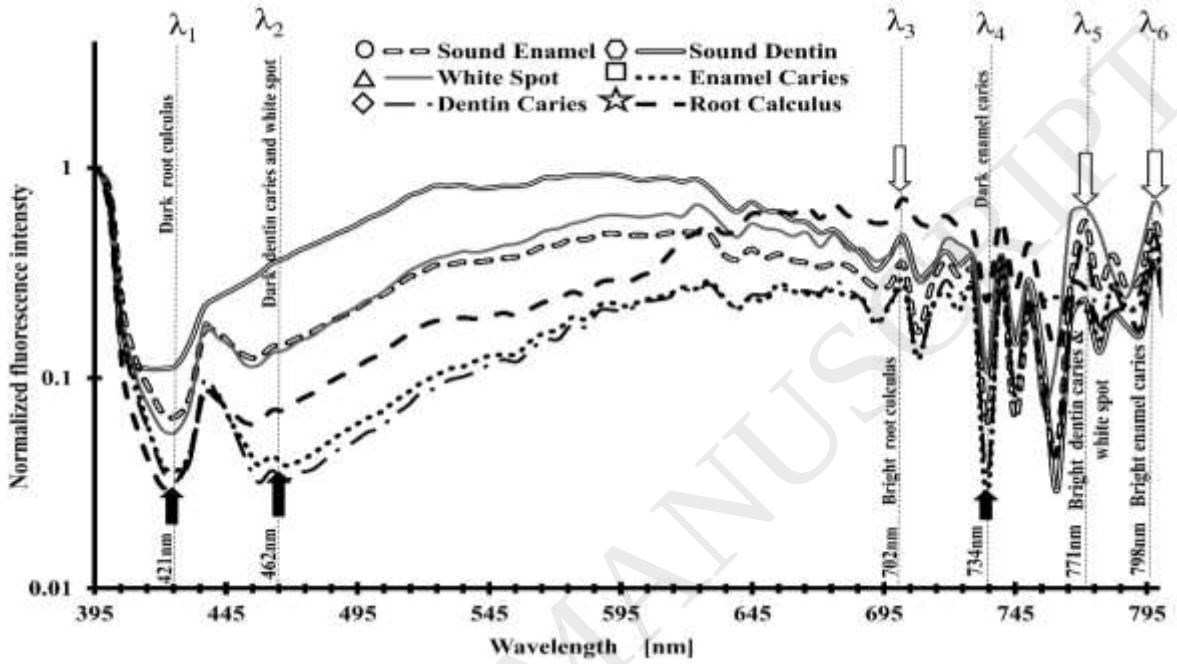

Fig. 3 Normalized fluorescence of dental classes, showing lower and higher peak wavelengths

Table 1 Various dental diseases contrast as a function of the obtained LIF wavelengths

Wavelength	White Spot	Root Calculus	Enamel Caries	Dentin Caries
λ_1 = 421 [nm]	___	Dark	___	___
λ_2 = 462 [nm]	Dark	___	___	Dark
λ_3 = 702 [nm]	___	Bright	___	___
λ_4 = 734 [nm]	___	___	Dark	___
λ_5 = 771 [nm]	Bright	___	___	Bright
λ_6 = 798 [nm]	___	___	Bright	___

However, in the presence of the excitation wavelength 395-nm, the difference in intensities between the various abnormal classes were not quite obvious. In order to enhance the differentiation between the illustrated diagnosed classes for the whole set of teeth specimen, another form of demonstrating the data as an absolute reflectance values through subtraction, and normalization of the original data from the dark frame and the calibration frame respectively, was attempted for a better class identification (Fig. 2). Afterwards, a logarithmic function was performed on the absolute reflectance values, targeting the

enhancement of the intensity presentation. Also, exposing the wavelengths distinguishing the 4 teeth pre-diagnosed abnormalities, according to low, and high peak intensity values (Fig. 3). Thus, presenting the tooth lesions as dark, or bright in appearance, when viewed in the 2-D image by normal eye vision.

Wavelengths corresponding to the high, and low intensity peaks representing the 6 tooth classes (Fig. 3) are demonstrated in Table 1. These peaks are revealing each of the tooth abnormality appearance either bright or dark according to the high, or low peak that it represents, respectively. The wavelengths related to the high peaks listed in the table are λ_3 = 702 nm, λ_5 = 771 nm, and λ_6 = 798 nm**,** at which the root calculus, white spot and dentin caries, and enamel caries are of bright manifestation respectively. While, at λ_1 = 421 nm, λ_2 = 462 nm, and λ_4 = 734 nm, the root calculus, white spot, dentin caries, and enamel caries have the least intensity peaks. Thus, they are seen dark.

B. Hyperspectral two-dimension outcomes

The grayscale 2-D images are the second form of results presented by the hyperspectral imaging process. These images are generated through applying the estimated wavelengths obtained from the one-dimensional hypercube outcomes presenting a visible form of lesion diagnosis. In which, each image of the exemplar pre-selected samples represented the 4 tooth abnormality classes at these estimated wavelengths. Each tooth disease was shown as either dark or bright in appearance (Fig. 4).

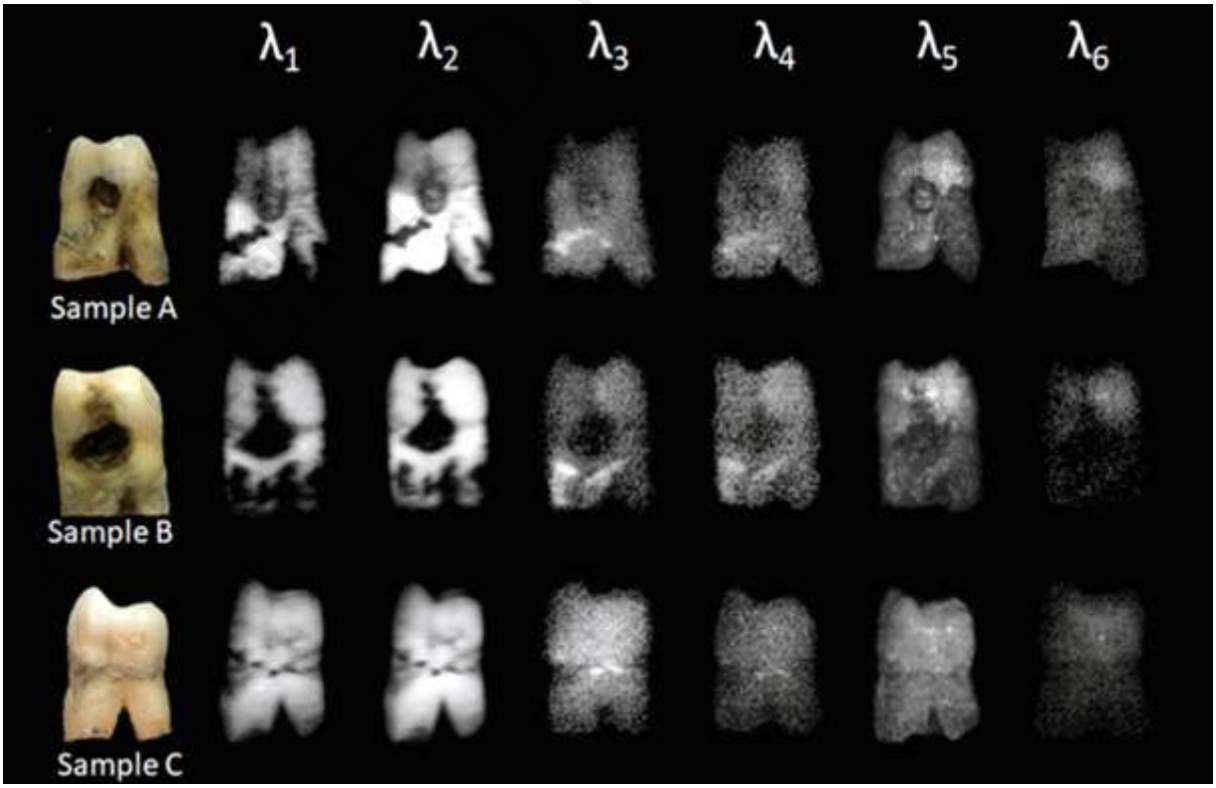

Fig. 4 Hyperspectral visualization of dental abnormalities for three modeled samples acquired at the estimated wavelengths

Images from the 3 pre-nominated samples showed the root calculus at λ_1 = 421 nm, as the darkest portion in comparison with other diagnosed abnormalities. Meanwhile, those obtained at λ_2 = 462 nm revealed that both white spot and dentine caries (noted in the color images Fig. 2) were much darker with respect to other diseases. At λ_3 = 702 nm, the root calculus appeared to be brighter, while the images at λ_4 = 734 nm, showed the enamel caries to be in its darkest appearance only for sample A, and B. It should be noted that for λ_5 = 771 nm**,** the images exhibit how bright are the white spot and dentin caries with respect to other maladies. Albeit, for λ_6 = 798 nm, the enamel caries tended to appear much brighter for sample A, and B, with a significant brightness of the white spot for all three presented samples.

Discussion

Hyperspectral imagining (HSI), noted as image spectrometer is considered as one of the most recent techniques evolved in the past decade for medical applications, especially in disease diagnosis and image-guided surgery [28]. HSI is an emerging imaging modality, with the advantage of being effective, non-invasive optical imaging technique. Moreover, it associates the possibilities presented by spectroscopic techniques, coupled with that of digital imaging. While being able to produce a three-dimensional dataset called hypercube, consisting of two spatial dimensions and one spectral dimension. Those spatially resolved spectral images, provide a diagnostic information map about the tissue physiology, morphology, and composition, by means of a series of information about tissue constituent and their spatial distribution from the point of view of each pixel spectral signature in the hyperspectral cube [27, 29].

Therefore, the utilization of hyperspectral camera in an imaging system based on laser induced fluorescence (LIF), and diffuse reflectance can enlighten the biomedical composition changes of the dental hard tissues throughout showing the different levels of the existent fluorophores[30].

This study presents a custom designed hyperspectral imaging system, employing a 395-nm laser diode source, and a simple optical system consisting of a beam expander, and a 90° quartz prism, for the purpose of normal light distribution over the irradiated tooth sample. The rationale behind using such excitation wavelength lies in its novelty to the field of laser induced fluorescence, and its low price. Moreover, its ability to gather the advantages offered by any commonly used UV source, as well as the features provided by the visible laser sources. Since, it is located in the far UV- near visible spectrum, therefore, it is capable of elaborating high fluorescence emission, that is produced from endogenous, and exogenous fluorophores upon exciting for the purpose of laser induced fluorescence [31]. Altogether, with the advantages of being a visible, with minimal thermal and mechanical damage as any other visible source. The fluorescence

emission in simultaneous with the diffuse reflectance produced from the examined tooth sample, were collected through a hyperspectral camera of type (SOC710). The obtained spatial, and spectral information from each irradiated tooth were reconstructed and displayed in the form of 1-D, 2-D, and 3-D dataset.

Benefiting from the hyperspectral imaging results, primarily, the one-dimensional pixel intensity with respect to the spectral band, each normal and abnormal dental class area, were demonstrated by a number of pixels precisely chosen according to a pre -diagnosis performed by a single experienced dentist for the 12 samples. The assimilated pixels representing each class were then formulated, and averaged, to be illustrated all together for further processing (Fig. 2). Averaging the pixel intensities for each individual wavelength, over the entire spectral band is to eliminate the huge intensity difference. Such variation in fluorescence intensity and spectral signature of the chosen pixels for each class over the whole 12 samples, was due to the diversity of tooth morphology, and the degree of demineralization, or to the grade of tooth caries development, together with the anisotropic nature of the tooth surface.

Clearly, the raw data curve (Fig. 2) showed the sound enamel and dentin auto fluorescence emission spectra with a small, narrow peak intensity centered at 436 nm, and a broad high peak one centered at 493-nm, due to the emission from natural endogenous fluorophores. In contrast, the 4 abnormality classes showed the same peak intensity attitude, albeit with lower fluorescence emission at these wavelengths, with an additional low intensity peaks centered around 771-nm, shifted towards the far visible red band and the near IR spectrum, demonstrating the fluency of the white spot and root calculus diseases over the entire sound classes. The occurrence of such low fluorescence intensity peaks is due to the presence of exogenous fluorophores, created from various bacteria species, and its bio-wastes[32].

Thence, the three main fluorescence peaks of the pre-diagnosed 6 classes, were λ=436 nm, λ=493 nm, and λ=771 nm. At those peaks, an observation of the existence of a medium intensity difference between classes was noticed, like the one shown between the normal dentin and root calculus and dentin caries at λ=436 nm, and λ=493 nm. While a least significant difference between the sound enamel and the white spot was detected at the same two fluorescence peaks due to the minor presence of exogeneous porphyrins. However, an apparent difference was found between the enamel caries and both the sound enamel and white spot classes at λ=436 nm, and λ=493 nm, because of its progressive lesion status. Explicitly, at λ=771 nm the intensity of the white spot lesion ruled over the entire examined phenotype intensity classes, due to the increased amount of diffuse reflectance and fluorescence emission arising from the bio-waste produced from the bacteria presence in the chalky demineralized areas, with respect to the emission produced from sound layers molecules.

In order, to improve differences between the classes, especially those concerning the dental abnormalities, for better discrimination, raw dataset $R(\lambda)$ of each class was normalized and represented as reflectance values. This normalizing process of each class dataset $S(\lambda)$ was achieved by subtracting and dividing each

data representing a class by the dark $D(\lambda)$, and calibration frame $C(\lambda)$ respectively, that was obtained prior measurements, equation (1).

$$S(\lambda) = \frac{R(\lambda) - D(\lambda)}{C(\lambda) - D(\lambda)} \qquad (1)$$

A logarithmic function was then applied to the normalized reflectance intensities, for smoothing, and moreover, to enhance the addressing of an accepted intensity differences between dental abnormalities classes, corresponding to the different wavelengths of the spectral band (Fig. 3). From which, a selection of wavelengths representing the maximum noticed intensity differences at low, and high peaks were identified. These low, and high peaks were then noted by being bright or dark. Bright wavelengths λ_3 = 702 nm, λ_5 = 771 nm, and λ_6 = 798 nm notified the wavelengths where the root calculus, white spot &dentine caries, and enamel caries classes appears to have high intensity peak respectively. Meanwhile, the 4 abnormality classes appeared dark at wavelengths, λ_1 = 421 nm, λ_2 = 462 nm, and λ_4 = 734 nm, in which, the root calculus, white spot and dentin caries, and enamel caries, exhibited low peak intensities.

Exploring the hyperspectral results *via* the 2-D images produced at the estimated wavelengths representing the high (bright), and low (dark) intensity peaks (Table 1). These images provided a visible map for the four pre-diagnosed dental lesions, especially the white spot and root calculus, and revealing how the four lesions appeared as dark or bright in the image with respect to other abnormality classes, according to the pre-selected wavelength, (Fig. 4).

Obviously, the spectral grayscale map introducing the 3 exemplar samples at the deduced wavelengths (Fig.4) provided a demonstration for the abnormality discrimination, in which, at λ_1 = 421 nm the three selected samples exhibited the same appearance whereas, the root calculus appeared darker than any other abnormality. Except for sample B, there was no difference between the root calculus and the dentin caries owing to the tremendous degree of dentin caries, causing a low exhibition of fluorescence intensity. For λ_2 = 462 nm, white spot lesion appeared darker with respect to the surrounding sound enamel for the three samples, while the dentin caries exhibited a dark intensity behavior with respect to the sound dentin for sample A, and a much more darker appearance for sample B. While, at λ_3 = 702 nm, it was obvious that the root calculus class showed the strongest brightness compared to all other lesions. Although λ_4 = 734 nm, is a wavelength considered to be in the far visible and near the IR band, the enamel caries appeared to be darker than the sound enamel class in sample A and B. For λ_5 = 771 nm, a tremendous bright appearance of the white spot with respect to the sound enamel, as well as other abnormalities in the 3 exemplar samples, also, the dentin caries have a bright distinctive appearance with respect to the cavity embracing it at A, and B. Respectively, λ_6 = 798 nm provides an image, illustrating the bright appearance of the enamel caries with

respect to the adjacent sound enamel, however by a less degree of brightness difference, when compared to the white spot lesion in sample A, and B.

Therefore, λ_3 = 702 nm, λ_5 = 771 nm were considered to be a key wavelength offering a single diagnoses of root calculus and white spot respectively with respect to other dental classes. Providing a reliable assessment diagnostic tool for those kinds of dental diseases. Finally, images produced by the wavelengths in the visible band, λ_1 = 421 nm, λ_2 = 462 nm, revealed that root calculus, and white spot and dentin caries are to be dark with respect to the sound enamel, and dentin classes. While, images at near IR wavelengths λ_3 = 702 nm, λ_5 = 771 nm, and λ_6 = 798 nm, except λ_4 = 734 nm, provides a bright form of the root calculus, white spot and dentin caries, and enamel caries, with respect to each other and moreover with respect to sound enamel, and dentin. Such result can be explained in regards to that when demineralized enamel and root calculus was excited by wavelengths in the UV- near visible spectrum, a fluorescence emission occurred in the far red, near infra-red spectrum, due to the increased presence exogenous fluorophores of various bacterial specimen [33].

The 1-D, and 2-D analysis obtained from the hypercube processing can offer a spectral map of the selective wavelengths, giving a reasonable diagnosis for the different hard tissue dental lesions, especially the early demineralization of the enamel layer, as well as the root calculus in the dentin layer.

Employing the obtained wavelengths into the design of a tunable digital or optical filter can provide the core of implementing a simple, effective, and non-invasive optical diagnostic tool for dental examination in the future. Such low-cost imaging system is built by a laser diode source, capable of producing fluorescence from the tooth under examination. It irradiates the tooth through a simple optical system, to ensure suitable irradiation and energy dissipation. The produced fluorescence, and reflectance from the morphology of the tooth surface are collected as images by a commonly used intra-oral camera. The collected stream of images or snap shots are then displayed and processed by a software installed to a computer connected directly to the camera.

To ensure high quality images, with reasonable signal to noise ratio, the specification of the intra-oral camera has to fulfil, or proportionally fulfil the same general characterization of the hyperspectral camera in use at the selected wavelengths, through guarantying high quantum efficiency QE(λ) [34] . Equation 2 emphasizes how to obtain quantum efficiency by standard methods [35].

$$\mathrm{QE}(\lambda) = \frac{electron}{pHotons} = \frac{DN(\lambda) \times \mathrm{hc} \times K_e}{I_{peak} \times t \times \lambda \times A_{pixel}} \qquad (2)$$

DN (λ) is the digital number of the averaged dark subtracted pixels within the spectral bands, and K_e is the conversion gain of the sensor, while I_{peak} is the peak photon intensity, t the integration time and A_{pixel} the pixel area.

This kind of system design can facilitate the diagnosis of white spot, and root calculus, which are considered as two of the most difficult lesions diagnosed currently under visible, non-hazardous irradiation, unlike IR hyperspectral imaging techniques, employing infra-red illumination of unknown thermal and mechanical effects on the tooth under examinations [36, 37]. It should be noted that the proposed custom hyperspectral imaging system cannot be compared to the commercially used VistaProof device, as the Vista-Proof utilize a 405-nm blue laser for irradiation, additionally of using a CCD camera for collecting the produced fluorescence images *in-vivo*, followed by a software for image signal processing to perform a color classification at only 2 wavelengths quantifying red and green components, giving a lesion severity meter ranged from 0 to 4 with high performance in detecting and quantifying dental plaque, and tartar over smooth areas, as well as an aiding tool to improve early diagnosis of white spot [38]. In contrast, our custom designed system utilizes a 395-nm UV- near visible wavelength for irradiation of tooth *in-vitro*, and the produced fluorescence are collected by a hyperspectral camera for the intension of obtaining cut-off wavelengths, discriminating different dental diseases especially white spot, and root calculus.

Finally, this study presents the foundation for the design of a simple, low cost, real-time, non-invasive, and non-hazardous diagnostic tool, based on a newly used UV-Visible diode laser source of minimal or no thermal and mechanical damage to the irradiated tooth. The collected stream of images, or individual snapshots, from the implemented digital or optical filter tuned to the selected wavelengths corresponding to abnormality classes. Those reconstructed and processed images can offer dentists a friendly, easy to use optical assessment diagnostic tool, with the advantage of figuring out the suspected areas within the tooth by white spot, and root calculus lesions. Furthermore, another form of enhancement can be introduced, by processing the images using a custom made 2-D Hilbert transform algorithm to define the enamel and dentin caries degree status, for precise, and less pain caries removal[39].

Conclusion

The proposed fluorescence hyperspectral imaging system presented herein employs a low power, newly used UV-visible laser diode source of wavelength 395-nm, characterized of gathering both features offered by both bands, altogether with minimal thermal and mechanical effects on the examined tooth. It has the capability of producing tooth auto-fluorescence, through a simple optical system. The hyperspectral camera, and its associated HSAnalysis2XL software was used to collect and reconstruct the produced tooth fluorescence emission. Providing lesion wavelengths from the 1-D outcomes, that were able to reveal each dental lesion distinctively, and presenting it visually as a 2-D image.

The system presents a set of estimated wavelengths referring to each of the dental abnormality, offering a potential assessment diagnostic tool for dentists to distinguish between different dental lesions, especially white spot, and root calculus that are difficult to diagnose under normal visual tactile, and other optical imaging techniques using visible laser sources.

Nevertheless, such a technique needs to be further tuned in terms of studying the effect of irradiating the curved surfaces of the tooth and its corresponding refractive indexes, in addition to decreasing the specular reflectance due to background, to enhance the quality of the produced images, as well as providing it with an image signal processing algorithm for producing a colored image, aiding in better quantification of different tooth classes.

Wavelengths distinguishing each abnormal class, especially the ones noting the root calculus at λ_3 = 702 nm, and the white spot at λ_5 = 771 nm can be the core for the design of a simple optical imaging system, made of a CCD, or intra-oral camera, equipped by a 395-nm diode laser source, and a set of optical or digital filters tuned to those lesion wavelengths, equipped altogether with pre-designed image signal algorithms. Such a simple, low cost, safe opto-imaging system can generate a series of reconstructed images, providing the dentist by a non-invasive, easy to use diagnostic tool, with the ability of detecting and quantifying the suspected tooth lesions and ultimately eliminating or decreasing any surgical interference of caries removal.

Acknowledgments

We are grateful for Prof. Mohamed A. Farag, College of Pharmacy, Cairo University, and Dr. Hany Abd-Elkhalek, Architecture Engineering Department, Military Technical College, for editing an earlier version of this manuscript.

References

1. Shetty, S. and M. Bailey. *A physical rendering model for human teeth*. in *ACM SIGGRAPH 2010 Posters*. 2010. ACM.
2. Ten Cate, A., *Oral Histology: Development, Structure, And Function. Saint Louis: Mosby.* Year Book, 5th edition. ISBN 0-8151-2952-1, 1998.
3. Selwitz, R.H., A.I. Ismail, and N.B. Pitts, *Dental caries.* The Lancet, 2007. **369**(9555): p. 51-59.
4. Petersen, P.E., *The World Oral Health Report 2003: continuous improvement of oral health in the 21st century–the approach of the WHO Global Oral Health Programme.* Community Dentistry and oral epidemiology, 2003. **31**(s1): p. 3-24.
5. Fejerskov, O. and E. Kidd, *Dental caries: the disease and its clinical management*. 2009: John Wiley & Sons.
6. Kidd, E. and O. Fejerskov, *What constitutes dental caries? Histopathology of carious enamel and dentin related to the action of cariogenic biofilms.* Journal of dental research, 2004. **83**(1_suppl): p. 35-38.

7. Murdoch-Kinch, C.A. and M.E. McLEAN, *Minimally invasive dentistry.* The Journal of the American Dental Association, 2003. **134**(1): p. 87-95.
8. Walsh, L., *The current status of low level laser therapy in detistry. Part 2. Hard tissue applications.* Australian dental journal, 1997. **42**(5): p. 302-306.
9. Bottenberg, P., et al., *Decision-making and preventive non-surgical therapy in the context of a European Core Curriculum in Cariology.* European Journal of Dental Education, 2011. **15**(s1): p. 32-39.
10. Bader, J.D., D.A. Shugars, and A.J. Bonito, *A systematic review of the performance of methods for identifying carious lesions.* Journal of public health dentistry, 2002. **62**(4): p. 201-213.
11. Dong, C., B. Cleghorn, and M. Hewko, *Shedding New Light on Early Caries Detection.* Journal of the Canadian Dental Association, 2008. **74**(10).
12. Angmar-Månsson, B. and J. Ten Bosch, *Optical methods for the detection and quantification of caries.* Advances in Dental Research, 1987. **1**(1): p. 14-20.
13. Brinkman, J., J. Ten Bosch, and P. Borsboom, *Optical quantitation of natural caries in smooth surfaces of extracted teeth.* Caries research, 1988. **22**(5): p. 257-262.
14. Hall, A. and J. Girkin, *A review of potential new diagnostic modalities for caries lesions.* Journal of Dental Research, 2004. **83**(1_suppl): p. 89-94.
15. El-Sharkawy, Y.H. and A.F. El Sherif, *Photoacoustic diagnosis of human teeth using interferometric detection scheme.* Optics & Laser Technology, 2012. **44**(5): p. 1501-1506.
16. El-Sharkawy, Y. *Detection and Characterization of Human Teeth Caries Using 2D Correlation Raman Spectroscopy*. Journal of Biomedical Physics and Engineering 2016.
17. Wenzel, A., et al., *Accuracy of visual inspection, fiber-optic transillumination, and various radiographic image modalities for the detection of occlusal caries in extracted non-cavitated teeth.* Journal of dental research, 1992. **71**(12): p. 1934-1937.
18. El-Sharkawy, Y.H., *Design and implementation of noninvasive laser imaging system for human teeth carious detection and removal.* Journal of Dental Lasers, 2015. **9**(2): p. 80.
19. Schneiderman, A., et al., *Assessment of dental caries with digital imaging fiber-optic transllumination (DIFOTITM): in vitro Study.* Caries Research, 1997. **31**(2): p. 103-110.
20. Sundström, F., et al., *Laser-induced fluorescence from sound and carious tooth substance: spectroscopic studies.* Swed Dent J, 1985. **9**(2): p. 71-80.
21. Lee, Y.-K., *Fluorescence properties of human teeth and dental calculus for clinical applications.* Journal of Biomedical Optics, 2015. **20**(4): p. 040901.
22. Zhang, L., L.Y. Nelson, and E.J. Seibel, *Red-shifted fluorescence of sound dental hard tissue.* Journal of Biomedical Optics, 2011. **16**(7): p. 071411.
23. Hibst, R. and R. Paulus. *New approach on fluorescence spectroscopy for caries detection*. in *Lasers in Dentistry V*. 1999. International Society for Optics and Photonics.
24. Van der Veen, M., et al., *Red autofluorescence of dental plaque bacteria.* Caries research, 2006. **40**(6): p. 542-545.
25. Fried, D., et al., *Nature of light scattering in dental enamel and dentin at visible and near-infrared wavelengths.* Applied optics, 1995. **34**(7): p. 1278-1285.
26. Betrisey, E., et al., *Caries diagnosis using light fluorescence devices: VistaProof and DIAGNOdent.* Odontology, 2014. **102**(2): p. 330-335.
27. Calin, M.A., et al., *Hyperspectral imaging in the medical field: present and future.* Applied Spectroscopy Reviews, 2014. **49**(6): p. 435-447.
28. Wolfe, W.L., *Introduction to imaging spectrometers*. Vol. 25. 1997: SPIE Press.
29. Lu, G. and B. Fei, *Medical hyperspectral imaging: a review.* Journal of biomedical optics, 2014. **19**(1): p. 010901.

30. Roblyer, D.M., et al., *Multispectral optical imaging device for in vivo detection of oral neoplasia.* Journal of biomedical optics, 2008. **13**(2): p. 024019.
31. Chen, Q., et al., *Quantitative method to assess caries via fluorescence imaging from the perspective of autofluorescence spectral analysis.* Laser Physics, 2015. **25**(8): p. 085601.
32. Walsh, L.J. and F. Shakibaie, *Ultraviolet-induced fluorescence: shedding new light on dental biofilms and dental caries.* Australasian dental practice, 2007. **18**(6): p. 56-60.
33. Borisova, E., T. Uzunov, and L. Avramov, *Laser-induced autofluorescence study of caries model in vitro.* Lasers in Medical Science, 2006. **21**(1): p. 34-41.
34. Luthman, A.S., et al., *Fluorescence hyperspectral imaging (fHSI) using a spectrally resolved detector array.* Journal of biophotonics, 2017. **10**(6-7): p. 840-853.
35. Bohndiek, S.E., et al., *Comparison of methods for estimating the conversion gain of CMOS active pixel sensors.* IEEE Sensors Journal, 2008. **8**(10): p. 1734-1744.
36. Usenik, P., et al., *Automated classification and visualization of healthy and diseased hard dental tissues by near-infrared hyperspectral imaging.* Applied Spectroscopy, 2012. **66**(9): p. 1067-1074.
37. Zakian, C.M., I.A. Pretty, and R. Ellwood, *Near-infared hyperspectral imaging of teeth for dental caries detection.* Journal of Biomedical Optics, 2009. **14**(6): p. 064047.
38. Rodrigues, J., et al., *Light-emitting diode and laser fluorescence-based devices in detecting occlusal caries.* Journal of biomedical optics, 2011. **16**(10): p. 107003.
39. Gawad, A.L.A., Y.H. El-Sharkawy, and A.F. El-Sherif, *Classification of human teeth caries using custom non-invasive optical imaging system.* Lasers in Dental Science, 2017. **1**(2-4): p. 73-81.